Cancer Letters 554 (2023) 216011

Contents lists available at ScienceDirect

Cancer Letters

journal homepage: www.elsevier.com/locate/canlet

Saikosaponin A enhances Docetaxel efficacy by selectively inducing death of dormant prostate cancer cells through excessive autophagy

Jiling Feng [a,b,c,h,1], Zhichao Xi [b,c,1], Xue Jiang [b,c], Yang Li [b,c], Wan Najbah Nik Nabil [b,c,d], Mengfan Liu [b,c], Zejia Song [b,e], Xiaoqiong Chen [b,c], Hua Zhou [a], Qihan Dong [f,g,**], Hongxi Xu [a,b,c,*]

[a] Shuguang Hospital Affiliated to Shanghai University of Traditional Chinese Medicine, No. 528, Zhangheng Road, Shanghai, 201203, China
[b] School of Pharmacy, Shanghai University of Traditional Chinese Medicine, No. 1200, Cailun Road, Shanghai, 201203, China
[c] Engineering Research Center of Shanghai Colleges for TCM New Drug Discovery, No. 1200, Cailun Road, Shanghai, 201203, China
[d] Pharmaceutical Services Program, Ministry of Health, Petaling Jaya, Selangor, 46200, Malaysia
[e] Faculty of Medicine, University of Turku, Kiinamyllynkatu 10, FI-20520, Turku, Finland
[f] Chinese Medicine Anti-Cancer Evaluation Program, Greg Brown Laboratory, Central Clinical School and Charles Perkins Centre, Faculty of Medicine and Health, The University of Sydney, Sydney, NSW, 2006, Australia
[g] Department of Endocrinology, Royal Prince Alfred Hospital, Sydney, NSW, 2050, Australia
[h] Precision Research Center for Refractory Diseases, Institute for Clinical Research, Shanghai General Hospital, Shanghai Jiao Tong University School of Medicine, Shanghai, 201620, China

ARTICLE INFO

Keywords:
Quiescent cancer cells
Prostate cancer
SSA
Induce autophagy
Akt

ABSTRACT

Quiescent cancer cells (QCCs), also known as dormant cancer cells, resist and survive chemo- and radiotherapy, resulting in treatment failure and later cancer recurrence when QCCs resume cell cycle progression. However, drugs selectively targeting QCCs are lacking. Saikosaponin A (SSA) derived from *Bupleurum* DC., is highly potent in eradicating multidrug-resistant prostate QCCs compared with proliferative prostate cancer cells. By further exacerbating the already increased autophagy through inactivation of Akt-mTOR signaling, SSA triggered cell death in QCCs. Contrarily, inhibition of autophagy or activation of Akt signaling pathway prevented SSA-induced cell death. The multicycle of Docetaxel treatments increased the proportion of QCCs, whereas administering SSA at intervals of Docetaxel treatments aggravated cell death *in vitro* and led to tumor growth arrest and cell death *in vivo*. In conclusion, SSA is posed as a novel QCCs-eradicating agent by aggravating autophagy in QCCs. In combination with the current therapy, SSA has potential to improve treatment effectiveness and to prevent cancer recurrence.

1. Introduction

Quiescent cancer cells (QCCs) are a subpopulation of cancer cells that reversibly arrest at G_0 phase. QCCs evade chemotherapies that target active proliferating cancer cells [1]. Survived QCCs can re-enter cell cycle, leading to cancer recurrence and metastasis [2,3]. The three proposed QCCs-targeted strategies are (i) blocking QCCs from re-entering the cell cycle, (ii) promoting QCCs entering cell cycle to regain sensitivity to chemotherapeutics, and (iii) eradication of QCCs in the G_0 state. While the second strategy has been thought to be risky,

Abbreviations: Baf, Bafilomycin A1; 5-FU, Fluorouracil; LAMP1, Lysosome-associated membrane protein 1; LC3, Microtubule- associated protein1 light chain 3; p62, SQSTM1/p62; PI, Propidium iodide; QCCs, Quiescent cancer cells; rps6, S6 Ribosomal Protein; SSA, Saikosaponin A; TUNEL, TdT-mediated dUTP Nick End Labeling.

* Corresponding author. Shuguang Hospital affiliated to Shanghai University of Traditional Chinese Medicine, No. 528, Zhangheng Road, Shanghai, 201203, China.

** Corresponding author. Faculty of Medicine and Health, The University of Sydney, Sydney, NSW, 2006, Australia.

E-mail addresses: fjlfreda@shutcm.edu.cn (J. Feng), xizhichao@shutcm.edu.cn (Z. Xi), jiangxue96@shutcm.edu.cn (X. Jiang), liyangsh1991@163.com (Y. Li), najbah@yahoo.com (W.N. Nik Nabil), mengfanliu@shutcm.edu.cn (M. Liu), Chenxiaoqiong92@163.com (X. Chen), zhouhua@shutcm.edu.cn (H. Zhou), qihan.dong@sydney.edu.au (Q. Dong), hxxu@shutcm.edu.cn (H. Xu).

[1] The authors contributed equally to this work.

https://doi.org/10.1016/j.canlet.2022.216011
Received 31 January 2022; Received in revised form 24 June 2022; Accepted 16 November 2022
Available online 26 November 2022

progress has been made under the first strategy: treatment with anti-estrogen therapy in breast cancer [4], and CDK4/6 inhibitors in pancreatic [5], liver [6] and brain tumors [7] are effective in maintaining dormancy and preventing tumor growth and metastasis. However, QCCs-targeting agents for eradication are still lacking.

Macroautophagy (hereafter referred as autophagy) is an evolutionally conserved mechanism and critical for tumor cell survival by degrading and recycling organelles and misfolded proteins to ensure energy balance. Preclinical studies have revealed that an increased autophagic activity facilitates cancer cells to enter quiescent state [8], which protects cells against chemotherapeutic stress and confers their survival [9,10]. Although autophagy is confirmed as a survival mechanism for cells to transit from proliferative to quiescent state [9–13], the significance of autophagy equilibrium in QCCs survival is unclear.

In the present study, we demonstrated that autophagic activity was increased in the experimental model of QCCs. We further identified that Saikosaponin A (SSA), a small molecule from *Bupleurum* DC., broked the autophagy equilibrium in QCCs by increasing the already activated autophagy level, leading to cell death of QCCs. Administering SSA at intervals of Docetaxel treatments potentiates Docetaxel's therapeutic effect *in vitro* and *in vivo*. Thus, SSA may be considered as a potential anticancer candidate to optimize treatment outcome and hinder recurrence by breaking the autophagy equilibrium in QCCs.

2. Materials and methods

2.1. Chemicals and reagents

Saikosaponin A (B20146, ≥98% purity) was purchased from Shanghai Yuanye Bio-Tech Co. Ltd, dissolved in DMSO (543900, Sigma) and stored at −80 °C. Docetaxel (T1034), Taxol (T0968), 5-FU (T0984), Cisplatin (T1564) and Etoposide (T0132) were from Targetmol. Z-VAD-FMK (C1202), RIPA lysis buffer (P0013C) and protease inhibitor cocktail (P1005) were procured from Beyotime, China. SYBR Green (S-7563) was purchased from Life Technologies (Carlsbad, CA, USA). Bafilomycin A1 (10374), Torin-1 (17146) and MK-2206 (15705) were obtained from CSNpharm, Chicago, USA.

2.2. Cell lines and culture

Human prostate cancer cell lines LNCaP, PC-3 and DU145, human embryonic kidney-(HEK)-293T cells were obtained from the American Type Culture Collection (ATCC, Manassas, VA, USA). Human prostate stromal cell line WPMY-1 and human hepatocyte line HL7702 were acquired from Cell Bank of Chinese Academy of Sciences, China. LNCaP, PC-3, DU145 and HL7702 were cultured in RPMI 1640 medium (MB4374, Dalian Meilun Biotechnology Co. Ltd., +penicillin/streptomycin) supplemented with 10% fetal bovine serum (FBS, Biological Industries, 04-001-1 A CS). HEK-293T and WPMY-1 cells were cultured in DMEM (Dalian Meilun Biotechnology Co) supplemented with 10% FBS. All cells were maintained at 37 °C in a humidified atmosphere with 5% CO_2. Prostate cancer cells were synchronized at quiescence as previously described [14]. Briefly, LNCaP and DU145 cells were grown to 70–80% confluence and maintained in serum-free medium for another 7 days. PC-3 cells were plated as monolayer until it reached 100% confluence, then maintained in serum-free medium for another 3 days. All cell culture supplies were from Wuxi NEST Biotechnology Co. Ltd.

2.3. SYBR green assay

SYBR Green assay was performed according to previous protocol [14]. Proliferative LNCaP, DU145 (7×10^3 cells/well) and PC-3 (5×10^3 cells/well) were seeded in 96-well plates. The cells were cultured in complete medium for 72 h, with or without indicated concentrations of chemotherapy drugs and SSA. The same number of cells were kept as a baseline and stored at −80 °C. For assays on quiescent cells, LNCaP (8×10^3 cells/well), DU145 (1×10^4 cells/well) and PC-3 (5×10^4 cells/well) cells were seeded in 96-well plates and synchronized at quiescence. QCCs were then incubated with or without chemotherapy drugs or SSA at indicated concentrations for 24 h, the culture medium was aspirated and cells were kept at −80 °C. The same number of cells were also plated and synchronized, then kept at −80 °C as baseline. Treated cells and their corresponding baseline cells were incubated in the dark with 100 μl/well of lysis buffer containing 1‰ SYBR Green. Intensity of SYBR Green fluorescence was quantified using plate reader (PerkinElmer) with excitation at 485/20 nm and emission at 528/20 nm. IC_{50} values were calculated from dose–response curves using GraphPad Prism 5 (La Jolla, CA, USA).

2.4. Cell viability assay

Proliferative LNCaP (1×10^5 cells/well), DU145 (1.5×10^5 cells/well) and PC-3 (2×10^5 cells/well) cells were seeded in 6-well plates and cultured in complete medium with chemotherapy drugs or SSA at indicated concentrations for 72 h. For QCCs assay, LNCaP (2×10^5 cells/well), DU145 (3×10^5 cells/well) and PC-3 (1×10^6 cells/well) cells were seeded in 6-well plates and synchronized at quiescence. QCCs were then incubated with or without chemotherapy drugs or SSA at indicated concentrations. Cells were harvested, stained with 1% Fixable Viability Dye (65-0867-14, Thermo Fisher) in PBS at 4 °C for 20 min and then re-suspended with PBS. Cell viability was determined with flow cytometer (BD Biosciences, San Jose, CA, USA) and analyzed using FlowJo software (version VX). The LD_{50} values (50% lethal dose) were calculated from dose–response curves using GraphPad Prism 5 (La Jolla, CA, USA).

2.5. Propidium iodide/annexin V staining

LNCaP, PC-3 and DU145 cells were seeded in 6-well plates and synchronized at quiescence. QCCs were then incubated with SSA at various concentrations for indicated times. After washed with PBS, cells were incubated at room temperature with PI and Annexin V (C10625, Beyotime) for 15 min in the dark. Apoptotic cells were determined with flow cytometer (BD Biosciences, San Jose, CA) and analyzed using FlowJo software (version VX), and Annexin V-positive cells were regarded as apoptotic cells.

2.6. Flow cytometry with Ki-67 staining

Proliferative LNCaP, DU145 and PC-3 cells were seeded in 6-well plates and cultured in complete medium with Docetaxel or DMSO for 12–24 h. Cells were permeabilized with 0.1% Triton-PBS and blocked with 0.5% BSA-PBS for 30 min. Cells were then incubated overnight with Ki-67 antibody (Abcam, ab92353) and FITC- conjugated secondary antibody for 1 h before it was re-suspended in 200 μl PBS. Flow cytometry (BD Biosciences, San Jose, CA) assay was performed and analyzed using FlowJo software (version VX).

2.7. Immunoblotting

Cell pellets were lysed with ice-cold RIPA lysis buffer in the presence of protease inhibitor cocktail. Protein quantification, electrophoresis and transfer were performed according to previous protocol [15]. The antibodies (human specific) for immunoblotting were GAPDH (ab128915, Abcam), LC3B (7543, Sigma-Aldrich), while antibodies for Phospho-Akt (Ser 473, 4060), Akt (9272), Phospho-S6 Ribosomal Protein (Ser 235/236, 4858), S6 Ribosomal Protein (2317), SQSTM1/p62 (5114) were supplied by Cell Signaling Technology.

2.8. Transfection

AKT1 (AKT cDNA cloned into the GV358 vector, with GFP labeling) and empty vector (GV358) plasmid were purchased from Genechem and

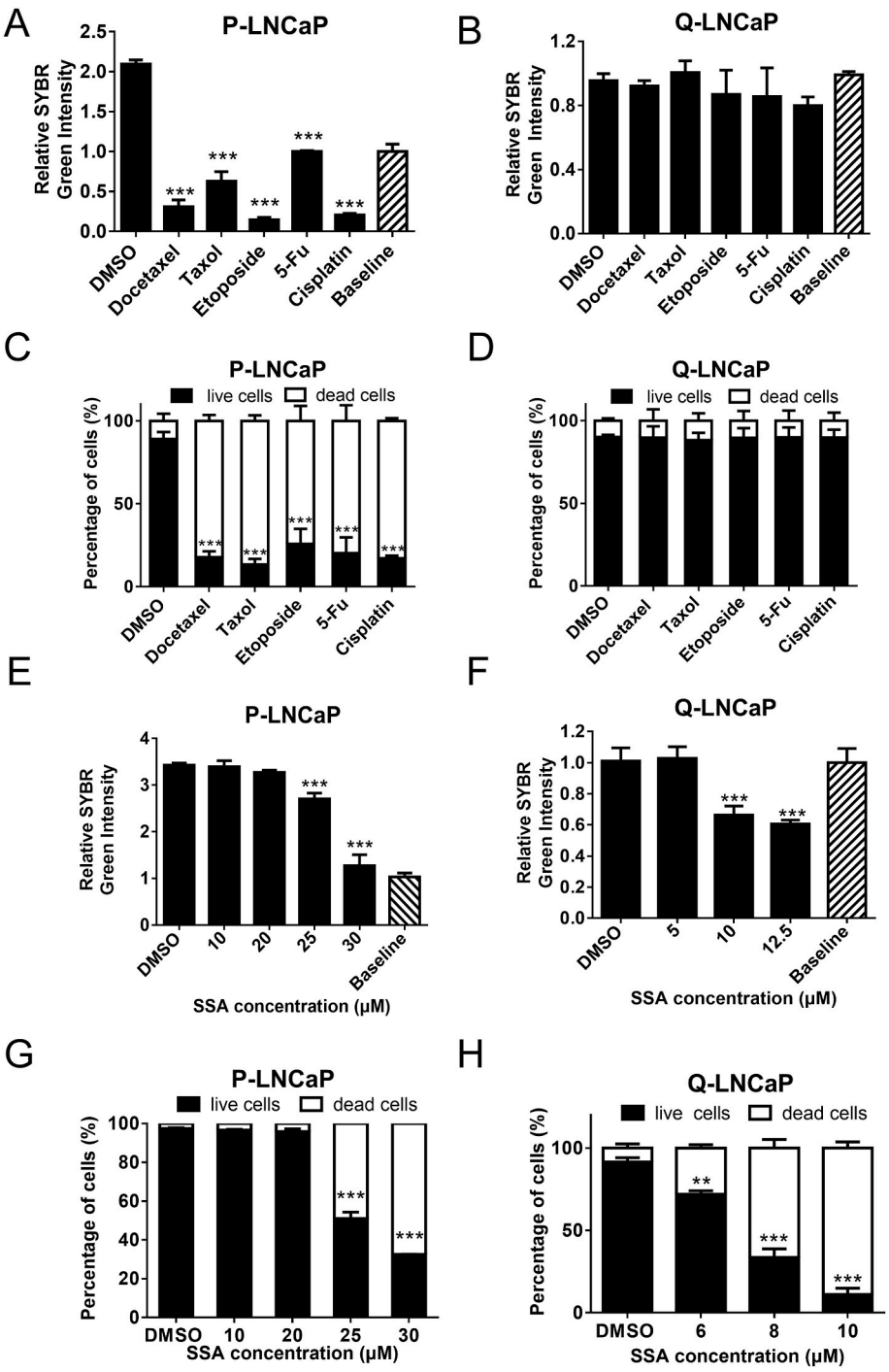

Fig. 1. SSA specifically induces cell death in chemo-resistant quiescent prostate cancer LNCaP cells. Proliferative (P) and quiescent (Q) LNCaP cells were treated with 5 chemotherapy drugs (40 μM) for 72 h, then subjected to SYBR Green assay (A, B) and cell viability assay (C, D). P- or Q- LNCaP cells were treated with SSA at the indicated concentrations and durations (72 h for P- cells, 24 h for Q-cells), then collected for SYBR Green assay (E, F). P- or Q- LNCaP cells were treated with SSA at the indicated concentrations and intervals (72 h for P- cells; 24 h for Q-cells), then collected for cell viability assay (G, H). Data are shown as mean ± S.D. of triplicate experiments, $^{**}p < 0.01$, $^{***}p < 0.001$.

transfected as manufacturer's instruction. (HEK)-293T cells were transfected with plasmid using a 2nd Generation Packaging System Mix (Lenti-PacTM HIV Expression Packaging Kit, GeneCopoeia, Changzhou, China). Virus were collected and stored in −80 °C. Prostate cancer cells were seeded in 24-well plates and infected with AKT1 lentivirus and GFP-LC3 lentivirus (Genechem, China) for 72 h. Cells with high GFP protein expression were then selected.

2.9. Immunofluorescence

Cells were fixed in 4% neutral-buffered paraformaldehyde in PBS for 15 min followed by permeabilization with 0.01% Triton X-100 in PBS for 15 min at room temperature. Fixed preparations were blocked with 3% BSA in PBS for 1 h, then incubated with primary antibodies against LAMP1 (ab62562) or TRITC-dUTP Labeling Mixture (TUNEL assay kit, Dalian Meilun Biotechnology Co) at 4 °C overnight. The stained cells were washed and incubated with Alexa Fluor-conjugated secondary antibodies (Alexa Fluor 555 goat anti-mouse, Invitrogen, A21422) at room temperature for 3 h (omit this step for TUNEL assay). Images were captured using a fluorescence microscope (Olympus).

2.10. Animal experiments

Animal experiments were approved by the Shanghai University of Traditional Chinese Medicine and animal care was in accordance with the institutional guidelines (PZSHUTCM190531011). Four-week-old

Table 1
IC_{50} values of chemotherapy drugs on proliferative (P) and quiescent (Q) prostate cancer cells.

	LNCaP		PC-3		DU145	
	P	Q	P	Q	P	Q
Docetaxel	88.80 ± 5.30 nM	>40 μM	0.28 ± 0.01 nM	>40 μM	1.46 ± 0.04 nM	>40 μM
Taxol	379.81 ± 47.90 nM		1.25 ± 0.06 nM		12.37 ± 0.22 nM	
Etoposide	2.80 ± 0.82 μM		6.32 ± 0.98 μM		4.83 ± 0.58 μM	
5-FU	6.92 ± 1.36 μM		16.34 ± 1.75 μM		23.10 ± 2.11 μM	
Cisplatin	1.98 ± 0.18 μM		1.03 ± 0.09 μM		1.05 ± 0.03 μM	

IC_{50} (concentration of 50% proliferation inhibition) values were calculated based on the results of SYBR Green assay (Fig. 1B, Supplementary Fig. S1B, and Fig. S2) by using GraphPad Prism 5. IC_{50} values are shown as mean ± S.D. of triplicate experiments.

male BALB/c nude mice were sourced from the Experimental Animal Center of the Chinese Academy of Science (Shanghai, China) and kept in a pathogen-free environment. PC-3 cells (2×10^6) were injected subcutaneously into the right flank of each mouse. When tumor volume reached 300 mm^3, mice were randomly divided into 4 groups (6 mice per group): Vehicle, Docetaxel, SSA and Docetaxel-SSA combination group. Drugs were administered intraperitoneally for 3 cycles; each cycle lasts for 7 days. Docetaxel (5 mg/kg, dissolved in Tween 80: EtOH: saline = 20: 13: 67) was injected once daily on the first day of each cycle for Docetaxel group and combination group. SSA (7.5 mg/kg, dissolved in 2.5% castor oil, 2.5% ethanol in saline) was injected once daily on Day 2–7 of each cycle for SSA group and combination group. The vehicle group received once daily injection of solvent control of Docetaxel on Day 1, followed by solvent control of SSA on Day 2–7 of each cycle. Tumor volume and body weight were monitored every other day. After 21 days, mice were sacrificed, tumors and main organs were resected, photographed and weighed. Tumor volumes were calculated using: (length × width × height) × π/6.

2.11. Immunohistochemistry

Tumors were fixed in 10% neutral-buffered paraformaldehyde. Next, the samples were embedded in paraffin, stained with hematoxylin and eosin, TUNEL (Dalian Meilun Biotechnology Co, LTD). Finally, the sections were mounted with DPX Mountant (Sigma, 317616) for histological analysis.

2.12. Statistical analysis

All data are expressed as means ± S. D. of at least 3 independent experiments. Statistical analysis was performed using SPSS 21.0. Student's two-tailed *t*-test compared between two different groups, while ANOVA analysis with Fisher's LSD multiple comparison test were performed for multiple groups. Values of $^*p < 0.05$, $^{**}p < 0.01$ and $^{***}p < 0.001$ indicated statistically significant.

3. Results

3.1. Resistance of QCCs to common chemotherapy drugs

To demonstrate that quiescent prostate cancer cells are insensitive to chemotherapy, we compared the cytotoxicity of five commonly used chemotherapy drugs between proliferative and quiescent prostate cancer cells. Experimental quiescence was achieved through a 7-day serum withdrawal for LNCaP and DU145 cells or 3-day contact inhibition for PC-3 cells as previously described [14,16]. In non-synchronized proliferative prostate cancer cells, the DNA content in vehicle control had at least doubled after 72 h compared to baseline at 0 h (Fig. 1A, Supplementary Fig. S1A). As expected, the DNA content did not show a significant increase over the same period in quiescent prostate cancer cells (Fig. 1B, Supplementary Fig. S1B), confirming the non-proliferating state. All five chemotherapy drugs effectively inhibited proliferation and increased cell death in proliferative cells with IC_{50} values ranging from 0.28 nM to 23.1 μM (Fig. 1A, Supplementary Fig. S1A, Fig. S2 and Table 1). However, these chemotherapy drugs were minimally cytotoxic to quiescent prostate cancer cells, even at high concentration of 40 μM for 72 h (Fig. 1B, Supplementary Fig. S1B). Fixable Viability Dye was used to further distinguish live from dead cells. None of the chemotherapy drugs increased the fraction of dead cells in quiescent prostate cancer cells compared to vehicle control (Fig. 1D, Supplementary Fig. S1D), while a clear increased cell death in proliferative prostate cancer cells was noted (Fig. 1C, Supplementary Fig. S1C), indicating the resistance and survival of QCCs in the presence of most common chemotherapy drugs.

3.2. SSA specifically induces cell death of QCCs

To identify QCCs-targeting cytotoxic agents, we screened an Approved Drug Library (L 1000, Targetmol) that consisted about 1700 compounds on quiescent LNCaP cells. Less than 1% of the tested compounds significantly induced death in quiescent LNCaP cells and Saikosaponin A (SSA, Supplementary Fig. S3A) was one of the most effective candidates. SSA exerted remarkable cytotoxicity on quiescent prostate cancer cells (Fig. 1F, Supplementary Fig. S1F) and weakly cytotoxic to proliferative prostate cancer cells (Fig. 1E, Supplementary Fig. S1E) or non-cancerous cells (Supplementary Fig. S3B). Further results of cell viability assay showed that SSA treatment for 24 h at 7.07 ± 0.37 μM, 6.23 ± 0.11 μM and 7.22 ± 0.08 μM caused 50% of cell death (LD_{50} values) in quiescent LNCaP, PC-3 and DU145 cells, respectively (Fig. 1H, Supplementary Fig. S1H and Table 2). However, even when treated with 20 μM SSA for 72 h, less than 5% cell death occurred in proliferative prostate cancer cells (Fig. 1G, Supplementary Fig. S1G), prostate stromal cell line WPMY-1 and hepatocyte cell line HL7702 (Supplementary Fig. S3C). These data suggested that SSA is a promising selective cytotoxic agent on quiescent prostate cancer cells with minimal damage on non-cancerous cells.

3.3. Autophagy is activated in QCCs and further elevated by SSA treatment

In exploring the mechanism of SSA-induced death of quiescent prostate cancer cells, we first examined the occurrence of apoptosis with

Table 2
LD_{50} values of SSA on proliferative (P) and quiescent (Q) prostate cancer cells.

	LNCaP		PC-3		DU145	
	P (72 h)	Q (24 h)	P (72 h)	Q (24 h)	P (72 h)	Q (24 h)
SSA (μM)	28.09 ± 1.31	7.07 ± 0.37	20.47 ± 1.91	6.23 ± 0.11	22.72 ± 0.71	7.22 ± 0.08

LD_{50} values (50% lethal dose) were calculated based on the results of cell viability assay (Fig. 1G and H, Supplementary Figs. S1G and H) by using GraphPad Prism 5. LD_{50} values are shown as mean ± S.D. of triplicate experiments.

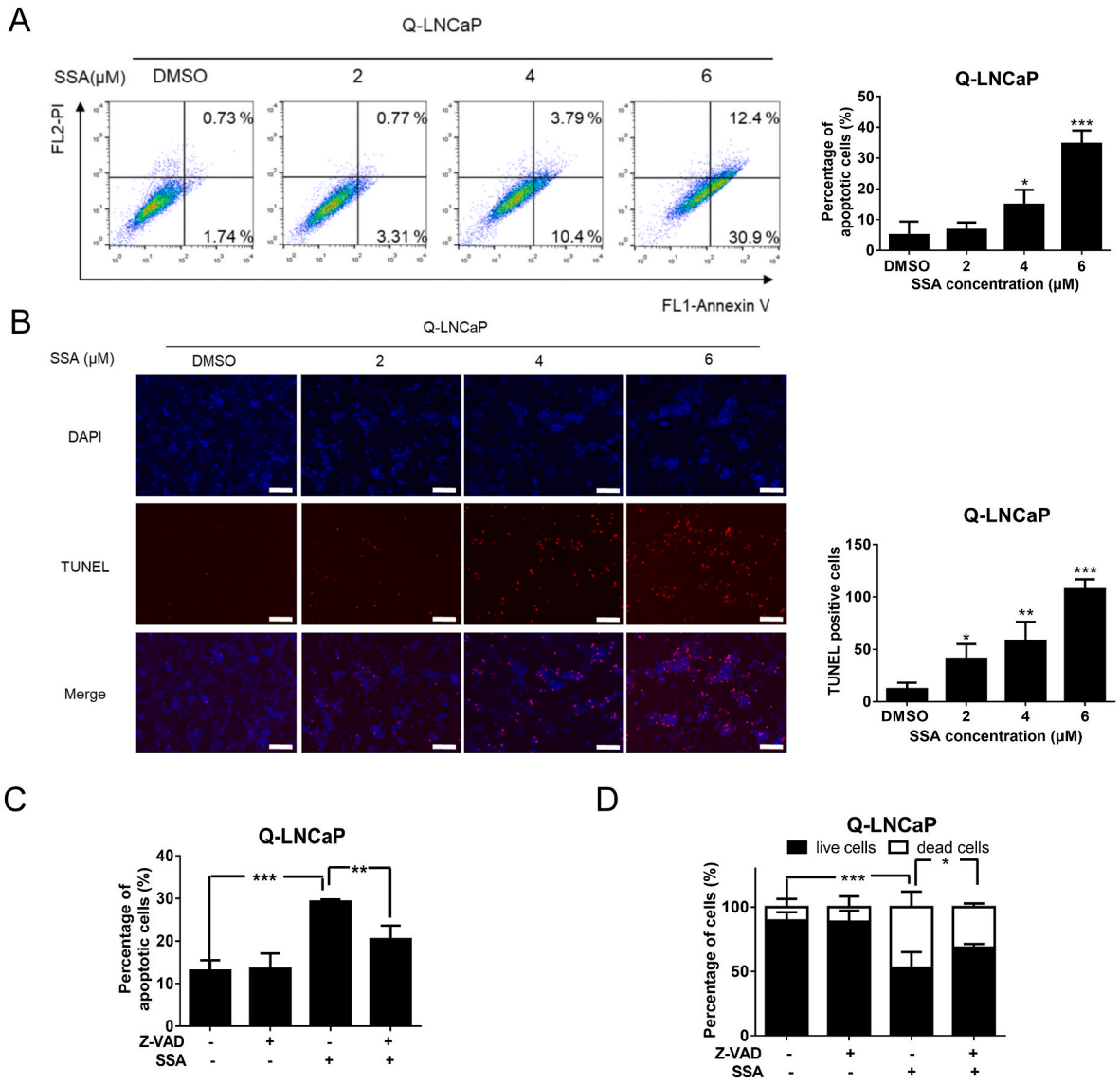

Fig. 2. SSA induces apoptosis in quiescent LNCaP cells. Quiescent LNCaP cells were treated with SSA at the indicated concentrations for 24 h. Cell apoptosis was detected by PI/Annexin V double staining (A) and TUNEL assay (B, scale bar: 100 μm). Statistical analysis was shown on the right. Q-LNCaP cells were pre-treated with or without Z-VAD-FMK (50 μM) for 2 h, and then exposed to SSA (LD_{50}) for another 24 h. Cell apoptosis (C) and cell viability (D) were measured using flow cytometry. Data are shown as mean ± S.D. of triplicate experiments, $^{*}p < 0.05$, $^{**}p < 0.01$, $^{***}p < 0.001$.

PI-Annexin V double staining assay. SSA dose-dependently induced apoptosis in quiescent LNCaP cells (Fig. 2A) and subsequentially confirmed by TUNEL assay (Fig. 2B). However, treating quiescent LNCaP cells with LD_{50} of SSA for 24 h caused only about 30% apoptosis (Fig. 2C). Pre-treatment with a pan-caspase inhibitor Z-VAD-FMK only partially rescued SSA-induced cell death (Fig. 2D). Similar discrepancies between overall cell deaths and apoptosis were also observed in quiescent PC-3 and DU145 cells (Supplementary Figs. S4 and S5).

We then evaluated the role of autophagy in SSA-induced cell death. Compared with proliferative LNCaP cells, the LC3 II/I ratio was increased and p62 protein level was decreased in quiescent LNCaP cells, indicative of autophagy induction in quiescent LNCaP cells (Fig. 3A). SSA treatment further aggravated the LC3 II/I ratio and the decline of p62 (Fig. 3A). We then detected the fusion of autophagosomes with lysosomes, a key step in autophagy, by examining the co-localization of GFP-LC3 and LAMP1. We constructed GFP-LC3-LNCaP and PC-3 stable cell line by lentivirus transfection, and performed immunofluorescence with anti-LAMP1 antibody. Compared with proliferative LNCaP cells, the GFP-LC3 puncta were increased in quiescent LNCaP cells and some of the puncta were well co-localized with LAMP1, which was further enhanced in the presence of SSA (Fig. 3B). Similar results were also observable in SSA-treated quiescent PC-3 cells (Supplementary Figs. S6A and B). Due to Atg 5 mutation, LC3 II was unnoticeable in DU145 cells [17], but p62 protein levels were decreased in quiescent DU145 and further reduced after SSA treatment (Supplementary Fig. S7A). These findings are consistent with the notion that increased autophagy may allow QCCs to survive but also raise an interesting scenario that a further increase in autophagy may lead to cell deaths.

3.4. An overactivated autophagy by SSA contributes to death of QCCs

To prove the concept that further enhancement of autophagy in QCCs may lead to cell death, we used autophagy inducer Torin-1 to mimic the scenario. Torin-1 indeed elevated LC3 II/I ratio, reduced p62 protein level and induced cell death in quiescent LNCaP cells (Fig. 3C–E). Combinatorial treatment with Torin-1 strengthened SSA-induced autophagy and cell death (Fig. 3C–E). We then applied Bafilomycin A1 (Baf) to block autophagosome-lysosome fusion. While Baf

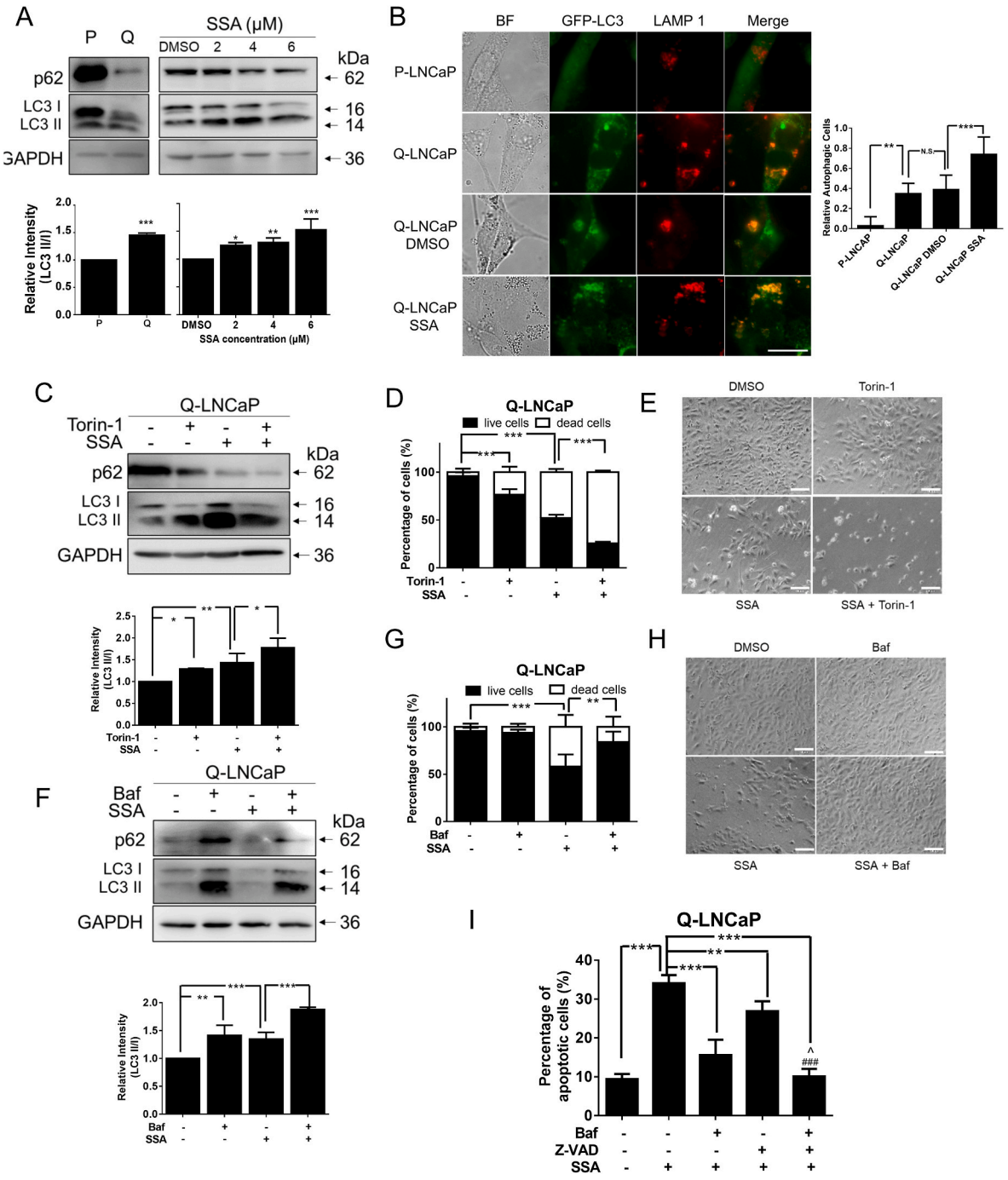

Fig. 3. Excessive autophagy induced by SSA plays a pivotal role in death of quiescent LNCaP cells. Immunoblotting (A) analyzed the expression of autophagy-related proteins in proliferative (P), quiescent (Q) LNCaP, and SSA-treated Q-LNCaP cells (2–6 μM) for 24 h. Relative LC3 II/I ratio was shown on the lower panel. Immunofluorescence analysis (B) of GFP-LC3 (green) and LAMP1 (red) co-localization in P-or Q- LNCaP cells treated with DMSO or SSA (LD_{50}) for 24 h, scale bar: 20 μm. Statistical analysis of relative autophagic cells was shown on the right. The yellow color in the merged image indicates co-localization, and was considered as autophagic cells. Q-LNCaP cells were pre-treated with or without Torin-1 (5 μM) or Bafilomycin A1 (2.5 μM) for 8 h, and then exposed to SSA (LD_{50}) for another 24 h. Cells were collected for immunoblotting (C, F, relative LC3 II/I ratio on the lower panel) and cell viability assay (D, G). GAPDH served as a loading control. Representative images are presented (E, H), scale bar: 100 μm. Cell apoptosis after treating with SSA alone or in combination with Bafilomycin A1 or Z-VAD-FMK or both was detected by PI/Annexin V double staining (I). Data are shown as mean ± S.D. of triplicate experiments. *: compared to SSA group; #: significance between Z-VAD-FMK + SSA and combination + SSA group; ^: significance between Bafilomycin A1+ SSA and combination + SSA group. */^ $p < 0.05$, ** $p < 0.01$, ***/### $p < 0.001$.

alone significantly increased both LC3 II/I ratio and p62 protein level in quiescent LNCaP cells, co-treatment of Baf and SSA escalated LC3 II/I ratio, recovered p62 and almost completely abolished SSA-induced cell death (Fig. 3F–H). These observations indicate that SSA is a potent autophagy flux inducer that triggers autophagic cell death in QCCs. Consistently, SSA-induced apoptosis was substantially rescued by Baf pre-treatment and Z-VAD-FMK rescued relatively small number of apoptotic cells compared with Baf. Together, co-treatment of Baf and Z-VAD-FMK nearly mitigated SSA-induced apoptosis (Fig. 3I), indicating that SSA-induced autophagy is mainly responsible for the occurrence of

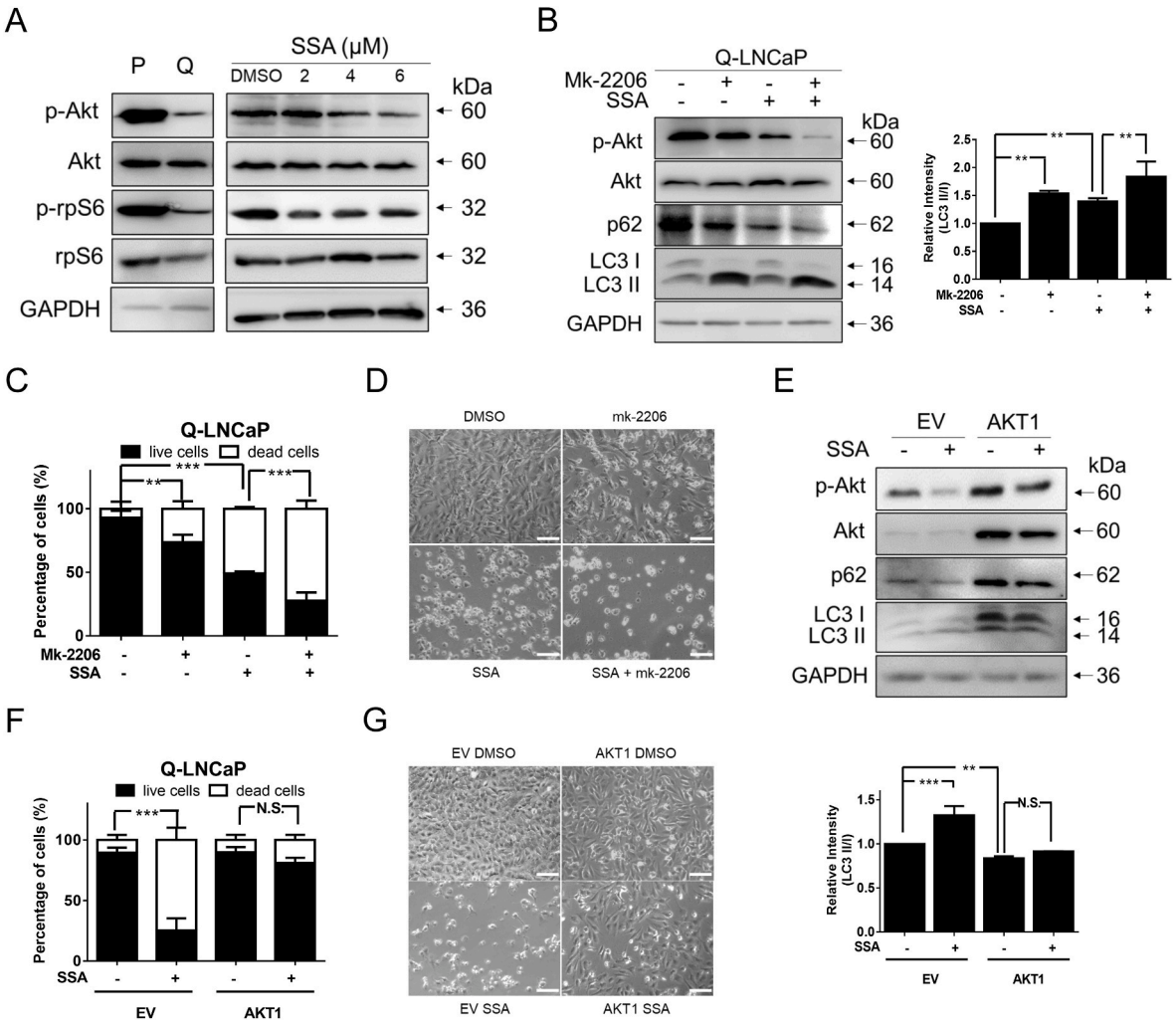

Fig. 4. SSA mediates autophagy in quiescent LNCaP cells through Akt-mTOR pathway. Immunoblotting (A) analyzed the expression of Akt signaling pathway related proteins in proliferative (P), quiescent (Q) LNCaP, and SSA-treated Q-LNCaP cells (2–6 μM) for 24 h. Q-LNCaP cells were pre-treated with or without MK-2206 (25 μM) for 2 h, and then exposed to SSA (LD_{50}) for another 24 h. Cells were collected for immunoblotting (B, relative LC3 II/I ratio on the right) and cell viability assay (C). Representative images are shown (D), scale bar: 100 μm. LNCaP cells that were stably transfected with AKT1-overexpressed plasmid (AKT1) or a parental empty vector (EV), were then treated with or without SSA (LD_{50} for WB; 10 μM for flow cytometry and images) for 24 h, respectively. Cells were collected for immunoblotting (E, relative LC3 II/I ratio on the lower panel) and cell viability assay (F). Representative images are shown (G), scale bar: 100 μm. Data are shown as mean ± S.D. of triplicate experiments, $^{**}p < 0.01$, $^{***}p < 0.001$, N.S., not significant. GAPDH served as a loading control.

apoptosis. SSA regulated autophagic cell death similarly in quiescent PC-3 and DU145 cell lines (Supplementary Figs. S6C–I, Supplementary Figs. S7B–H). These data indicate that excessive autophagy is responsible for SSA-induced death in quiescent prostate cancer cells.

3.5. Over-reduction of Akt/mTOR signaling increases SSA-induced QCCs cell death

We next examined the involvement of Akt/mTOR signaling pathway as a critical regulator of autophagy in maintaining survival of QCCs. The activation of Akt/mTOR signaling pathway was detected through phosphorylation of Akt and S6 Ribosomal Protein (rpS6) [18]. As expected, the Akt/mTOR activities were suppressed in autophagic quiescent prostate cancer cell lines. Phospho-Akt (Ser^{473}) and phospho-rpS6 ($Ser^{235/236}$) were down-regulated, while no significant changes in the Akt and rpS6 levels (Fig. 4A, Supplementary Fig. S8A and Fig. S9A). Notably, SSA dose-dependently further lowered the Akt/mTOR activity in quiescent LNCaP, PC-3 and DU145 cells (Fig. 4A, Supplementary Fig. S8A and Fig. S9A). Consistent with SSA-induced down-regulation of phospho-Akt and enhancement in autophagy, Akt inhibitor MK-2206 increased LC3 II/I ratio and induced quiescent LNCaP cell death (Fig. 4B–D). Concurrent exposure to MK-2206 and SSA for 24 h significantly expanded the percentage of dead quiescent LNCaP cells. Correspondingly, phospho-Akt and p62 levels were decreased and LC3 II/I ratio was further increased with the combined treatment than SSA alone (Fig. 4B–D). Similar results were also found in quiescent PC-3 and DU145 cell lines (Supplementary Figs. S8B–D, Supplementary Figs. S9B–D). Overall, SSA induces autophagy and cell death in QCCs plausibly through inhibition of the Akt/mTOR pathway, which is a negative regulator of autophagy.

3.6. SSA mediates autophagy through Akt/mTOR pathway

To verify the role of Akt in SSA-induced autophagy, we transfected prostate cancer cells with a plasmid containing full length AKT1 cDNA- or a parental empty vector. Protein expression of both Akt and phospho-Akt were significantly increased in AKT1-transfected cells (Fig. 4E, Supplementary Figs. S8E and S9E). Reduction of LC3 II/I ratio and upregulation of p62 indicated that autophagy was inhibited in quiescent LNCaP-AKT1 cells compared with empty vector-transfected cells. Treatment with SSA for 24 h significantly increased LC3 II/I ratio, decreased p62 and phospho-Akt in LNCaP-EV cells compared with the

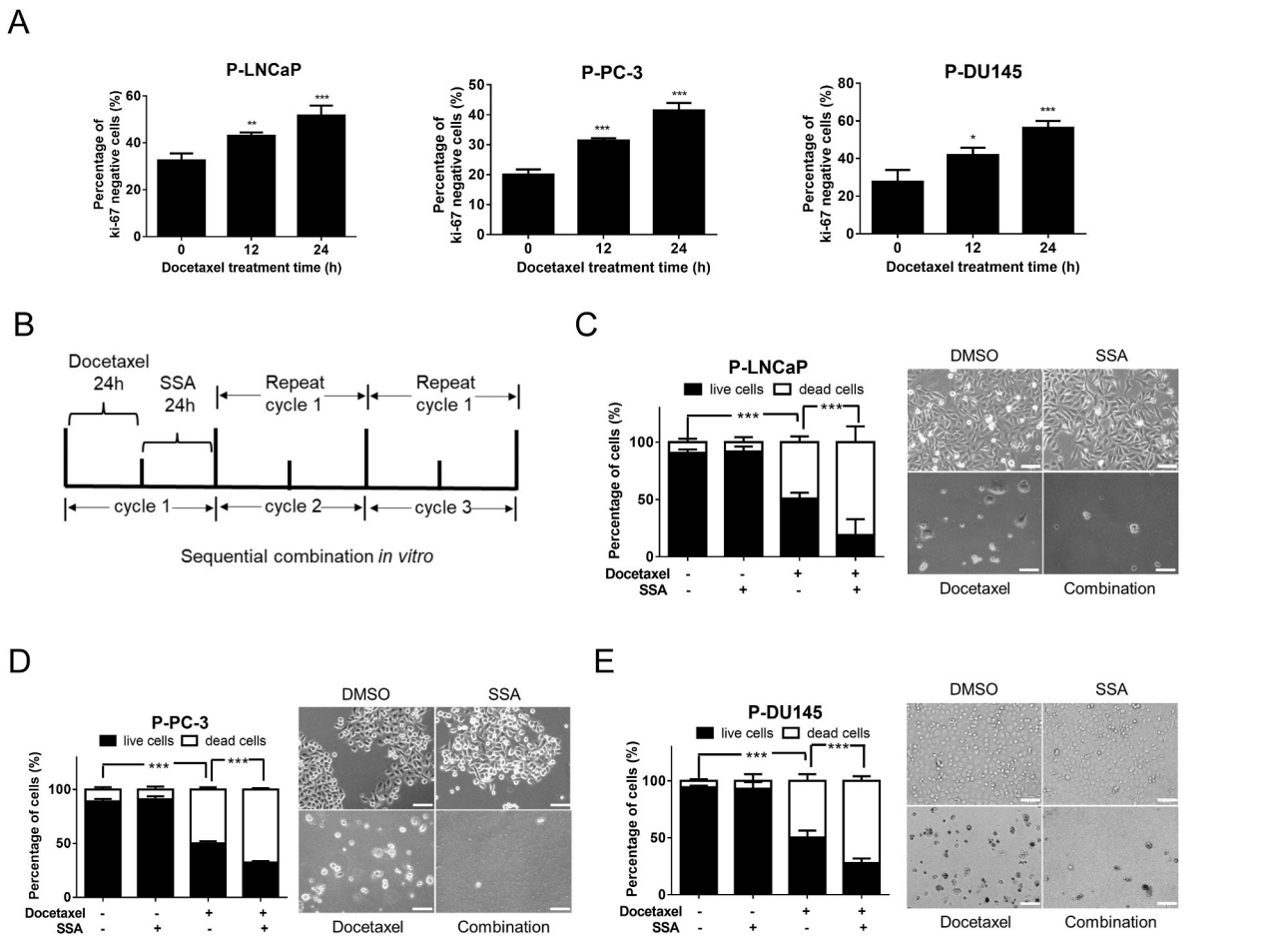

Fig. 5. SSA enhances chemosensitivity of Docetaxel *in vitro*. Proliferative LNCaP, PC-3 and DU145 cells were treated with Docetaxel (100 nM for LNCaP, 20 nM for PC-3 and 30 nM for DU145) for 0, 12, 24 h, respectively. Cells were harvested, stained with Ki-67 antibody, then subjected to flow cytometric assay (A). Schedule of sequential combination treatment *in vitro* (B). Cells were treated with Docetaxel and SSA (Docetaxel: 50 nM for LNCaP, 10 nM for PC-3 and 15 nM for DU145; SSA: 20 μM) according to the treatment schedule. Cell viability was assessed (left) and representative images of P- LNCaP (C), PC-3 (D) and DU145 (E) cells are shown (right, scale bar: 100 μm). Data are shown as mean ± S.D. of triplicate experiments, $*p < 0.05$, $**p < 0.01$, $***p < 0.001$.

change in LNCaP-AKT1 cells. We next examined whether Akt overexpression could rescue the cytotoxicity effect of SSA. Treatment with 10 μM SSA for 24 h caused more than 80% cell death in quiescent LNCaP-EV cells, but overexpression of Akt almost abolished the cytotoxicity effect of SSA (Fig. 4F and G). Similar findings were obtained in quiescent PC-3 and DU145 cells (Supplementary Figs. S8F and G and Supplementary Figs. S9F and G). Therefore, SSA-induced cell death of QCCs mainly depends on the Akt/mTOR-mediated autophagy.

3.7. Administering SSA at intervals of Docetaxel treatments enhances chemotherapeutic efficacy in vitro and in vivo

Since chemotherapy and radiotherapy primarily target rapidly proliferating cancer cells [19,20], we hypothesized that these treatments might cause accumulation of QCCs, which eventually contribute to therapy failure when they repopulate. Hence, we monitored the percentage of Ki-67 negative cells [21,22] in proliferating prostate cancer cells following exposure to Docetaxel for 0, 12 and 24 h, respectively. Docetaxel increased Ki-67 negative fraction time-dependently in all three prostate cancer cell lines (Fig. 5A). Considering the selective cytotoxicity of SSA on QCCs, we next evaluated the cytotoxic effects of combining Docetaxel with SSA in tandem (Fig. 5B). We chose 20 μM of SSA for the combination treatment based on its unapparent cytotoxicity in proliferative prostate cancer cells (Fig. 1E and G). Combination treatment for three sequential cycles significantly raise the percentage of dead prostate cancer cells, compared with SSA or Docetaxel alone (Fig. 5C–E).

To verify the finding *in vivo*, Docetaxel (5 mg/kg on Day 1 of a cycle) and SSA (7.5 mg/kg on days 2–7 of a cycle) were injected intraperitoneally when PC-3 xenograft tumor volume reached 300 mm^3 (Fig. 6A). Although Docetaxel or SSA treatment alone significantly suppressed tumor growth, the sequential combination further improved their treatment efficacy. Combination of Docetaxel and SSA not only retarded the tumor growth but also shrank the tumor size compared to the vehicle control group (Fig. 6B–D). Microscopically, tumor density was reduced and apoptosis was increased following combination treatment of Docetaxel and SSA (Fig. 6E). Importantly, we observed no significant change in mouse body weight in SSA treated group (Fig. 6F). The decreased body weight in combined treatment group was no difference statistically compared to Docetaxel alone.

4. Discussion

Tumors are heterogenous comprising both rapid proliferative and quiescent cancer cells. In the present study, we demonstrate, in three prostate cancer cell lines, that proliferative cancer cells are sensitive to chemotherapeutic drugs, but the experimental QCCs exert strong resistance to multiple chemotherapy agents. Since anti-cancer action of the most chemotherapy drugs are cell cycle dependent, QCCs residing at G_0 naturally evade the drug action. In addition, our results showed that the proportion of QCCs was time-dependently increased after Docetaxel treatment, indicating chemotherapy drugs may expand the fraction of

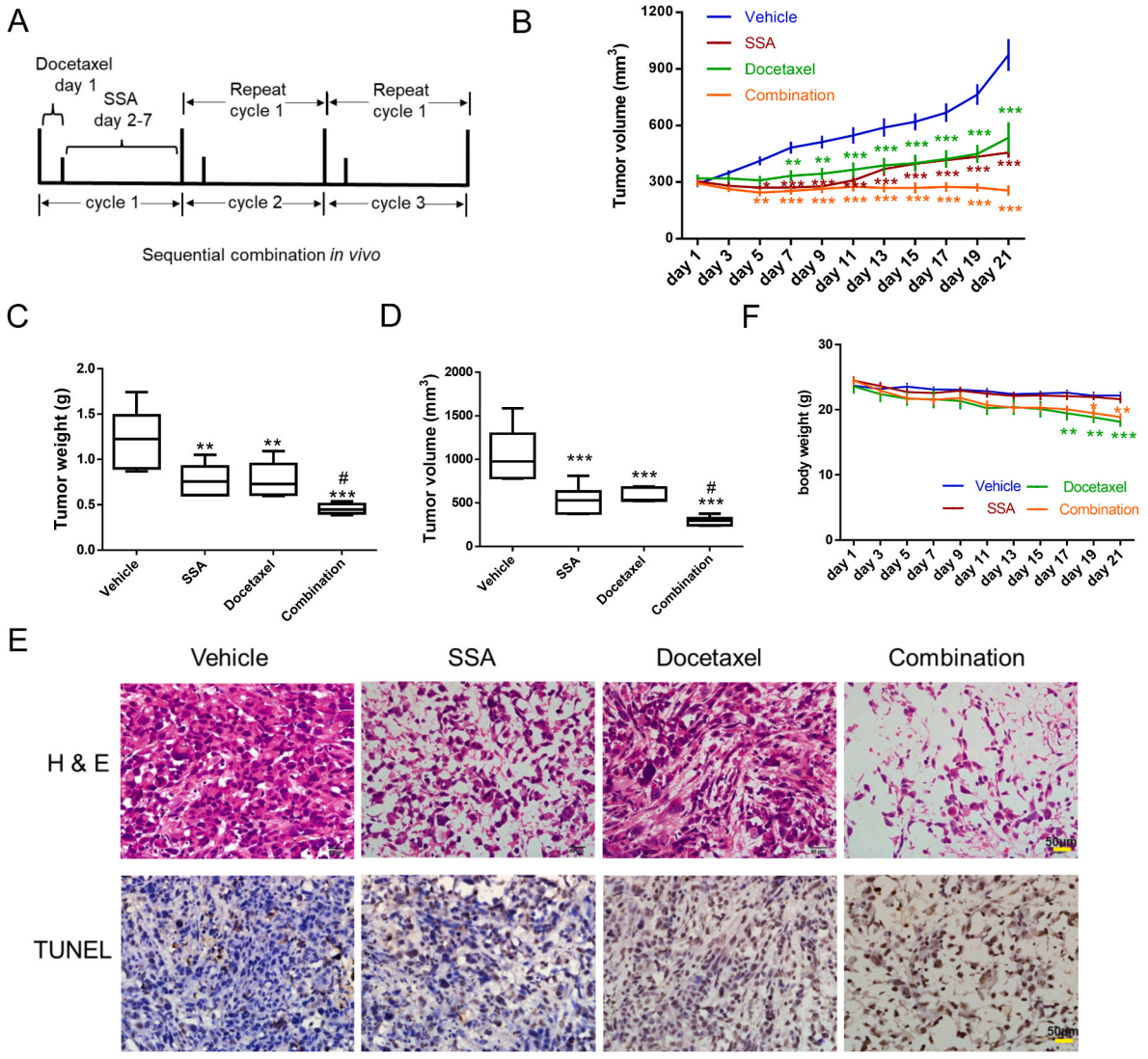

Fig. 6. SSA enhances chemosensitivity of Docetaxel *in vivo*. Nude mice were xenografted with PC-3 cells and randomly divided into 4 groups (n = 6). Tumor-bearing mice were then intraperitoneally treated with vehicle, SSA (7.5 mg/kg), Docetaxel (5 mg/kg) and SSA-Docetaxel combination as shown in treatment schedule (A). Tumor volume and body weight were recorded every other day (B and F). After 21 days of treatment, mice were sacrificed, the tumor weight (C) and volume (D) were measured. Data are shown as mean ± S.D. of 6 mice in each group, $^{*}p < 0.05$, $^{**}p < 0.01$, $^{***}p < 0.001$ (compared to vehicle group), $\#p < 0.05$ (compared to Docetaxel group). Representative images of H&E and TUNEL staining of tumors are shown (E), scale bar: 50 μm.

QCCs and contribute to drug resistance. These observations are consistent with the clinical findings that ovarian cancer cells isolated from avascular collagenous nodules were quiescent post-chemotherapy [23], while surviving QCCs and their repopulation led to chemotherapy resistance and cancer recurrence [24,25]. Tumors that were enriched with chemo-resistant quiescent cells relapsed significantly earlier than tumors with fewer QCCs [26]. Therefore, developing agents to eradicate multidrug-resistant QCCs is necessary to reduce the risk of cancer recurrence.

With the purpose to eradicating QCCs we screened more than 1700 compounds from the Approved Drug Library using the experimental model of QCCs, including drugs approved by Food and Drug Administration (FDA), European Medicine Agency (EMA), China Food and Drug Administration (CFDA) and other nations [27]. We identified that SSA could strongly induce cell death in QCCs but with limited effect on proliferative cancer cells. SSA is an approved drug by Pharmaceutical and Medical Devices Agency (PMDA, Japan), and an active ingredient in a Japanese traditional crude drug, Daisaikoto Extract [28]. Previous studies have shown that SSA possesses multiple bioactivities, including anti-inflammation, antioxidant, antifibrosis and immune-regulation [29–32]. The present study is the first time to report SSA cytotoxicity on QCCs. As a drug already approved for clinical use for other indications, the action and the mode of action of SSA on QCCs need to be clarified prior to its repurposing in clinical practice.

Autophagy is considered to contribute to drug resistance by protecting tumor cells from the cytotoxicity of chemotherapy drugs [33]. Thus, combined use of autophagy inhibitors and chemotherapy drugs may improve therapeutic outcomes and the autophagy inhibitor, hydroxychloroquine, has been investigated in anticancer clinical trials (NCT00786682, NCT01026844 and NCT00568880). Consistent with the notion that autophagy is activated in quiescent cancer cells [11,12,34], we found increased autophagy after synchronizing prostate cancer cells in quiescence state. However, by further enhancing autophagy, SSA treatment led to death of QCCs. These results suggest that autophagy equilibrium plays a vital role in QCCs survival, and inducing excessive autophagy can possibly become a potential strategy to eliminate QCCs. Cancer cells have been proposed to have defective autophagic capacities and inducing further autophagy has been shown to enhance anticancer effects [35]. For example, autophagy inducers such as rapamycin [36], metformin [37] and cepharanthine [38] have been studied pre-clinically

for their anticancer effects. Moreover, SSA significantly inhibited Akt/mTOR pathway, which negatively regulates autophagy. Overexpression of Akt almost abolished the cytotoxic effect, indicating Akt/mTOR pathway is required for the cytotoxic effect of SSA on QCCs. It worth noting that, although AKT inhibitor MK-2206 exerted cytotoxic effect on QCCs, its impact was not as strong as SSA. It remains to be determined whether SSA can also induce autophagy through other pathways.

It is interesting to note that DU145 cells have Atg 5 mutation [39], yet they remain responsive to SSA induced cell death. The possible explanations are as follows. Atg 5-deficient cell line may exert "alternative autophagy", in which cargos are engulfed by the *trans*-Golgi membrane 5 and degraded in autolysosomes by Unc-51-like kinase 1 (Ulk1), beclin 1 or wipi3 [40,41]. Furthermore, SSA exerted cytotoxicity in DU145 cells could also result from inhibition of Akt or its downstream pathways independent from autophagy [42].

Chemotherapy is commonly administered in cycles, as the intervals between cycles are vital for normal tissues to recover [43]. However, the intervals may also provide opportunity for QCCs to re-enter the cell cycle and to cause treatment failure [1]. Taking advantage of the selectivity of SSA in eradicating QCCs, this study tested the efficacy of introducing SSA at the intervals between cycles of Docetaxel treatments. This tandem combination evidently induced cell death of QCCs *in vitro*, and shrank the tumor volume *in vivo* when compared with Docetaxel or SSA alone. These findings lay a good foundation for applying selective QCCs-targeting drugs selectively targeting QCCs, such as SSA to improve outcome of chemotherapeutic drugs that mainly target proliferative cancer cells [44].

In conclusion, our data confirm the critical role of autophagy in QCCs survival, and SSA as a clinically approved drug can specifically induce cell death in QCCs by further exacerbating autophagy. Our findings suggest that combining chemotherapeutic agents that target proliferative cancer cells with SSA that eradicates QCCs, potentially prevent treatment failure and cancer recurrence.

Author contribution

Hongxi Xu and Qihan Dong supervised the project; Jiling Feng and Zhichao Xi drafted the manuscript; Jiling Feng, Xue Jiang, Mengfan Liu and Zejia Song performed the experiments; Xiaoqiong Chen and Wan Najbah Nik Nabil performed the statistical analyses; Yang Li and Hua Zhou revised the article. All authors read and approved the final article.

Funding

This work is supported by National Natural Science Foundation of China [grant numbers 81803571, 82104209]; Project funded by China Postdoctoral Science Foundation [grant number 2020TQ0198] and Key-Area Research and Development Program of Guangdong Province [grant number 2020B1111110003].

Declaration of competing interest

The authors have no conflicts of interest to declare.

Appendix A. Supplementary data

Supplementary data to this article can be found online at https://doi.org/10.1016/j.canlet.2022.216011.

References

[1] J.L. Mohler, E.S. Antonarakis, A.J. Armstrong, A.V. D'Amico, B.J. Davis, T. Dorff, et al., Prostate cancer, version 2.2019, NCCN clinical practice guidelines in oncology, J. Natl. Compr. Cancer Netw. 17 (5) (2019) 479–505.
[2] J.J. Kim, I.F. Tannock, Repopulation of cancer cells during therapy: an important cause of treatment failure, Nat. Rev. Cancer 5 (7) (2005) 516–525.
[3] J. Chen, Y. Li, T.S. Yu, R.M. McKay, D.K. Burns, S.G. Kernie, et al., A restricted cell population propagates glioblastoma growth after chemotherapy, Nature 488 (7412) (2012) 522–526.
[4] C. Davies, H. Pan, J. Godwin, R. Gray, R. Arriagada, V. Raina, et al., Long-term effects of continuing adjuvant tamoxifen to 10 years versus stopping at 5 years after diagnosis of oestrogen receptor-positive breast cancer: ATLAS, a randomised trial, Lancet 381 (9869) (2013) 805–816.
[5] A. Chou, D. Froio, A.M. Nagrial, A. Parkin, K.J. Murphy, V.T. Chin, et al., Tailored first-line and second-line CDK4-targeting treatment combinations in mouse models of pancreatic cancer, Gut 67 (12) (2018) 2142–2155.
[6] J. Bollard, V. Miguela, M. Ruiz de Galarreta, A. Venkatesh, C.B. Bian, M.P. Roberto, et al., Palbociclib (PD-0332991), a selective CDK4/6 inhibitor, restricts tumour growth in preclinical models of hepatocellular carcinoma, Gut 66 (7) (2017) 1286–1296.
[7] W.R. Wiedemeyer, I.F. Dunn, S.N. Quayle, J. Zhang, M.G. Chheda, G.P. Dunn, et al., Pattern of retinoblastoma pathway inactivation dictates response to CDK4/6 inhibition in GBM, Proc. Natl. Acad. Sci. U. S. A. 107 (25) (2010) 11501–11506.
[8] W.N. Nik Nabil, Z.C. Xi, Z.J. Song, L. Jin, X.D. Zhang, H. Zhou, et al., Towards a framework for better understanding of quiescent cancer cells, Cells 10 (3) (2021) 562.
[9] T. Shimizu, E. Sugihara, S. Yamaguchi-Iwai, S. Tamaki, Y. Koyama, W. Kamel, et al., IGF2 preserves osteosarcoma cell survival by creating an autophagic state of dormancy that protects cells against chemotherapeutic stress, Cancer Res. 74 (22) (2014) 6531–6541.
[10] R.J. Correa, Y.R. Valdes, T.M. Peart, E.N. Fazio, M. Bertrand, J. McGee, et al., Combination of AKT inhibition with autophagy blockade effectively reduces ascites-derived ovarian cancer cell viability, Carcinogenesis 35 (9) (2014) 1951–1961.
[11] L. Vera-Ramirez, S.K. Vodnala, R. Nini, K.W. Hunter, J.E. Green, Autophagy promotes the survival of dormant breast cancer cells and metastatic tumour recurrence, Nat. Commun. 9 (1) (2018) 1944.
[12] A. La Belle Flynn, B.C. Calhoun, A. Sharma, J.C. Chang, A. Almasan, W. P. Schiemann, Autophagy inhibition elicits emergence from metastatic dormancy by inducing and stabilizing Pfkfb3 expression, Nat. Commun. 10 (1) (2019) 3668.
[13] A. Carcereri de Prati, E. Butturini, A. Rigo, E. Oppici, M. Rossin, D. Boriero, et al., Metastatic breast cancer cells enter into dormant state and express cancer stem cells phenotype under chronic hypoxia, J. Cell. Biochem. 118 (10) (2017) 3237–3248.
[14] Z. Xi, M. Yao, Y. Li, C. Xie, J. Holst, T. Liu, et al., Guttiferone K impedes cell cycle re-entry of quiescent prostate cancer cells via stabilization of FBXW7 and subsequent c-MYC degradation, Cell Death Dis. 7 (6) (2016), e2252.
[15] Y. Li, Z. Xi, X. Chen, S. Cai, C. Liang, Z. Wang, et al., Natural compound Oblongifolin C confers gemcitabine resistance in pancreatic cancer by downregulating Src/MAPK/ERK pathways, Cell Death Dis. 9 (5) (2018) 538.
[16] X. Jiang, Y. Li, J.L. Feng, W.N. Nik Nabil, R. Wu, Y. Lu, et al., Safrana l prevents prostate cancer recurrence by blocking the Re-activation of quiescent cancer cells via downregulation of S-phase kinase-associated protein 2, Front. Cell Dev. Biol. 8 (2020), 598620.
[17] M.S. Lee, C.W. Tsai, C.P. Wang, J.H. Chen, H.H. Lin, Anti-prostate cancer potential of gossypetin via inducing apoptotic and autophagic cell death, Mol. Carcinog. 56 (12) (2017) 2578–2592.
[18] S. Saiki, Y. Sasazawa, Y. Imamichi, S. Kawajiri, T. Fujimaki, I. Tanida, et al., Caffeine induces apoptosis by enhancement of autophagy via PI3K/Akt/mTOR/p70S6K inhibition, Autophagy 7 (2) (2011) 176–187.
[19] C.P. Alves, I. Dey-Guha, S. Kabraji, A.C. Yeh, N.P. Talele, X. Sole, et al., AKT1(low) quiescent cancer cells promote solid tumor growth, Mol. Cancer Therapeut. 17 (1) (2018) 254–263.
[20] K.K. Payne, R.C. Keim, L. Graham, M.O. Idowu, W. Wan, X.Y. Wang, et al., Tumor-reactive immune cells protect against metastatic tumor and induce immunoediting of indolent but not quiescent tumor cells, J. Leukoc. Biol. 100 (3) (2016) 625–635.
[21] M. Sobecki, K. Mrouj, J. Colinge, F. Gerbe, P. Jay, L. Krasinska, et al., Cell-cycle regulation accounts for variability in ki-67 expression levels, Cancer Res. 77 (10) (2017) 2722–2734.
[22] M. Boldrini, C.A. Fulmore, A.N. Tartt, L.R. Simeon, I. Pavlova, V. Poposka, et al., Human hippocampal neurogenesis persists throughout aging, Cell Stem Cell 22 (4) (2018) 589–599, e5.
[23] Z. Lu, M.T. Baquero, H. Yang, M. Yang, A.S. Reger, C. Kim, et al., DIRAS3 regulates the autophagosome initiation complex in dormant ovarian cancer cells, Autophagy 10 (6) (2014) 1071–1092.
[24] N.D. James, M.R. Sydes, N.W. Clarke, M.D. Mason, D.P. Dearnaley, M.R. Spears, et al., Addition of docetaxel, zoledronic acid, or both to first-line long-term hormone therapy in prostate cancer (STAMPEDE): survival results from an adaptive, multiarm, multistage, platform randomised controlled trial, Lancet 387 (10024) (2016) 1163–1177.
[25] S. Yano, K. Takehara, H. Tazawa, H. Kishimoto, Y. Urata, S. Kagawa, et al., Cell-cycle-dependent drug-resistant quiescent cancer cells induce tumor angiogenesis after chemotherapy as visualized by real-time FUCCI imaging, Cell Cycle 16 (5) (2017) 406–414.
[26] I. Puig, S.P. Tenbaum, I. Chicote, O. Arqués, J. Martínez-Quintanilla, E. Cuesta-Borrás, et al., TET2 controls chemoresistant slow-cycling cancer cell survival and tumor recurrence, J. Clin. Invest. 128 (9) (2018) 3887–3905.
[27] J. Du, J. Shang, F. Chen, Y. Zhang, N. Yin, T. Xie, et al., A CRISPR/Cas9-Based screening for non-homologous end joining inhibitors reveals ouabain and penfluridol as radiosensitizers, Mol. Cancer Therapeut. 17 (2) (2018) 419–431.

[28] Y. Matsuo, K. Matsumoto, N. Inaba, Y. Mimaki, Daisaikoto inhibits pancreatic lipase activity and decreases serum triglyceride levels in mice, Biol. Pharm. Bull. 41 (9) (2018) 1485–1488.
[29] C.H. Piao, C.H. Song, E.J. Lee, O.H. Chai, Saikosaponin A ameliorates nasal inflammation by suppressing IL-6/ROR-gammat/STAT3/IL-17/NF-kappaB pathway in OVA-induced allergic rhinitis, Chem. Biol. Interact. 315 (2019), 108874.
[30] Y. Fu, X. Hu, Y. Cao, Z. Zhang, N. Zhang, Saikosaponin a inhibits lipopolysaccharide-oxidative stress and inflammation in Human umbilical vein endothelial cells via preventing TLR4 translocation into lipid rafts, Free Radic. Biol. Med. 89 (2015) 777–785.
[31] W.S. Wu, ERK signaling pathway is involved in p15INK4b/p16INK4a expression and HepG2 growth inhibition triggered by TPA and Saikosaponin a, Oncogene 22 (7) (2003) 955–963.
[32] J. Li, S. Wang, N. Wang, Z. Wang, Research advances of traditional Chinese medicine in cancer immunotherapy, Chin Med Cult 3 (2020) 245–253.
[33] R.K. Amaravadi, J. Lippincott-Schwartz, X.M. Yin, W.A. Weiss, N. Takebe, W. Timmer, et al., Principles and current strategies for targeting autophagy for cancer treatment, Clin. Cancer Res. 17 (4) (2011) 654–666.
[34] P. Baquero, A. Dawson, A. Mukhopadhyay, E.M. Kuntz, R. Mitchell, O. Olivares, et al., Targeting quiescent leukemic stem cells using second generation autophagy inhibitors, Leukemia 33 (4) (2019) 981–994.
[35] S. Ramachandran, I.S. Kaushik, S.K. Srivastava, Pimavanserin: a novel autophagy modulator for pancreatic cancer treatment, Cancers 13 (22) (2021) 5661.
[36] M.K. Koenig, C.S. Bell, A.A. Hebert, J. Roberson, J.A. Samuels, J.M. Slopis, et al., Efficacy and safety of topical rapamycin in patients with facial angiofibromas secondary to tuberous sclerosis complex: the TREATMENT randomized clinical trial, JAMA Dermatol 154 (7) (2018) 773–780.
[37] W.R. Cho, C.C. Wang, M.Y. Tsai, C.K. Chou, Y.W. Liu, Y.J. Wu, et al., Impact of metformin use on the recurrence of hepatocellular carcinoma after initial liver resection in diabetic patients, PLoS One 16 (3) (2021), e0247231.
[38] B.Y. Law, W.K. Chan, S.W. Xu, J.R. Wang, L.P. Bai, L. Liu, et al., Natural small-molecule enhancers of autophagy induce autophagic cell death in apoptosis-defective cells, Sci. Rep. 4 (2014) 5510.
[39] D.Y. Ouyang, L.H. Xu, X.H. He, Y.T. Zhang, L.H. Zeng, J.Y. Cai, et al., Autophagy is differentially induced in prostate cancer LNCaP, DU145 and PC-3 cells via distinct splicing profiles of ATG5, Autophagy 9 (1) (2013) 20–32.
[40] H. Yamaguchi, S. Honda, Wipi3 is essential for alternative autophagy and its loss causes neurodegeneration, Nat. Commun. 11 (1) (2020) 5311.
[41] Y. Nishida, S. Arakawa, K. Fujitani, H. Yamaguchi, T. Mizuta, T. Kanaseki, et al., Discovery of Atg5/Atg7-independent alternative macroautophagy, Nature 461 (7264) (2009) 654–658.
[42] S. Revathidevi, A.K. Munirajan, Akt in cancer: mediator and more, Semin. Cancer Biol. 59 (2019) 80–91.
[43] P. Board, Prostate Cancer Treatment (PDQ(R)), Patient Version – PDQ Cancer Information Summaries, 2002.
[44] H. Li, W.Y. Wei, H.X. Xu, Drug discovery is an eternal challenge for the biomedical sciences, Acta Materia Medica 1 (1) (2022) 1–3.